

Cooperative High-Temperature Spin Crossover Accompanied by a Highly Anisotropic Structural Distortion

Il'ya A. Gural'skiy,^{*,[ab]} Bohdan O. Golub,^[a] Sergii I. Shylin,^[ab] Vadim Ksenofontov,^[b] Helena J. Shepherd,^[c] Paul R. Raithby,^[c] Wolfgang Tremel^[b] and Igor O. Fritsky^[a]

Abstract: Spin transition is a spectacular example of molecular switching that can provoke extreme electronic and structural reorganizations in coordination compounds. A new 3D cyanoheterometallic framework $[\text{Fe}(\text{pz})\{\text{Au}(\text{CN})_2\}_2]$ has been synthesised. A highly cooperative spin crossover in this compound is observed at 367 K and 349 K in heating and cooling modes respectively. Mössbauer spectroscopy reveals a complete transition between diamagnetic and paramagnetic states of the iron centres. The low spin (LS) to high spin (HS) transition induces a drastic structural distortion that incorporates large one-directional expansion (ca. 10.6 %) and contraction (ca. 9.6 %) of the lattice. Negative thermal expansion along *c*-axis below and above transition temperature is detected.

Introduction

Among different switchable compounds, spin crossover (SCO) complexes possess a unique variety of accessible characteristics of transition behaviour related to a large set of organic/inorganic ligands for building coordination architectures.^[1–4] This crossover process is known for complexes of $3d^4 - 3d^7$ metal ions and it is related to the re-configuration of their electronic structures caused by the change of temperature, light excitation, pressure, magnetic field or guest effects.^[5] Practical achievements in the field of SCO include switchable nanomaterials^[6–11], composites^[12], displays^[13], electronic^[14,15] and mechanical^[16,17] elements, microthermometers^[18], chemical sensors^[19] etc. The development of novel compounds with a specific combination of transition temperature, abruptness, hysteresis and completeness of SCO

places significant demands on the synthetic chemistry. Most SCO complexes display SCO well below room temperature, although for some families of SCO materials transitions above room temperature are observed. Amongst the most commonly studied SCO systems with such high temperature transitions are iron(II) 1,2,4-triazolic and pyrazolylborate complexes.^[20,21] Unfortunately, complexes of the first family are very difficult to structurally characterize.^[22,23] Different complexes with the spin transitions above 400 K have been reported^[24–30], although they are often weakly cooperative and gradual in nature.

Iron containing cyanoheterometallic frameworks, including analogues of Hofmann clathrates^[31], are another family of intensively studied SCO materials that can possess bistability in a wide temperature range up to and above room temperature.^[32] They are also known for their sensitivity to the inclusion of guests into large guest accessible pores within a coordination framework.^[33–39] The variety of these SCO complexes is related to the different cyanometallates (Ni(II), Pd(II), Pt(II), Cu(I), Ag(I), Au(I), Cr(III), Nb(IV), etc.) and N-donor aromatic ligand (pyridines, pyrimidines, pyridazine, triazoles) that are suitable for the construction of these rigid polymeric structures.^[32]

In general, the LS \rightarrow HS transition is accompanied by an increase of Fe-N distances (by c.a. 10 %), as a result of the electronic transition within the *d*-shell - from nonbonding t_{2g} orbitals to antibonding e_g orbitals. This in turn leads to an expansion of the lattice of between 2 and 10 %. Indeed, these switchable structural properties have themselves attracted recent attention for use in mechanically active actuating devices.^[16,17] Thus an in-depth understanding of structural changes is not only essential to rationalising and improving functional properties in these systems, it is also key to the development of new applications.

Results and Discussion

In this paper we describe a route towards a novel iron(II)-gold(I) coordination framework $[\text{Fe}(\text{pz})\{\text{Au}(\text{CN})_2\}_2]$ **1** supported by bridging cyanide and pyrazine ligands. The crystal structure of **1** at 300 K is shown in **Figure 1**. **1** crystallizes in the orthorhombic space group *Fmmm*.

Cyanoheterometallic layers propagate in the *bc* plane and iron ions are coordinated by 4 cyanide groups that form their equatorial coordination environment. The iron is axially coordinated by bridging μ_2 -pyrazine ligands propagating the structure along the *a*-direction.

The potential pores in a sub-lattice of the framework are large, leading to interpenetration of two identical nets, connected through aurophilic interactions into a densely packed structure of

- [a] Dr. I.A. Gural'skiy, Mr. B.O. Golub, Mr. S.I. Shylin, Prof. I.O. Fritsky
Department of Chemistry
Taras Shevchenko National University of Kyiv
Volodymyrska St. 64, Kyiv 01601, Ukraine
E-mail: illia.guralskiy@univ.kiev.ua
http://physchem.univ.kiev.ua/fritsky/guralskiy_eng.html
- [b] Dr. I.A. Gural'skiy, Mr. S.I. Shylin, Dr. V. Ksenofontov, Prof. W. Tremel
Institute of Inorganic and Analytical Chemistry
Johannes Gutenberg University of Mainz
Staudingerweg 9, Mainz 55099, Germany
- [c] Dr. H.J. Shepherd, Prof. P.R. Raithby
Department of Chemistry
University of Bath
Claverton Down, Bath BA2 7AY, UK

Supporting information for this article is given via a link at the end of the document.

1. These aurophilic interactions also propagate along the *a*-direction with an Au...Au distance of 3.379 Å.

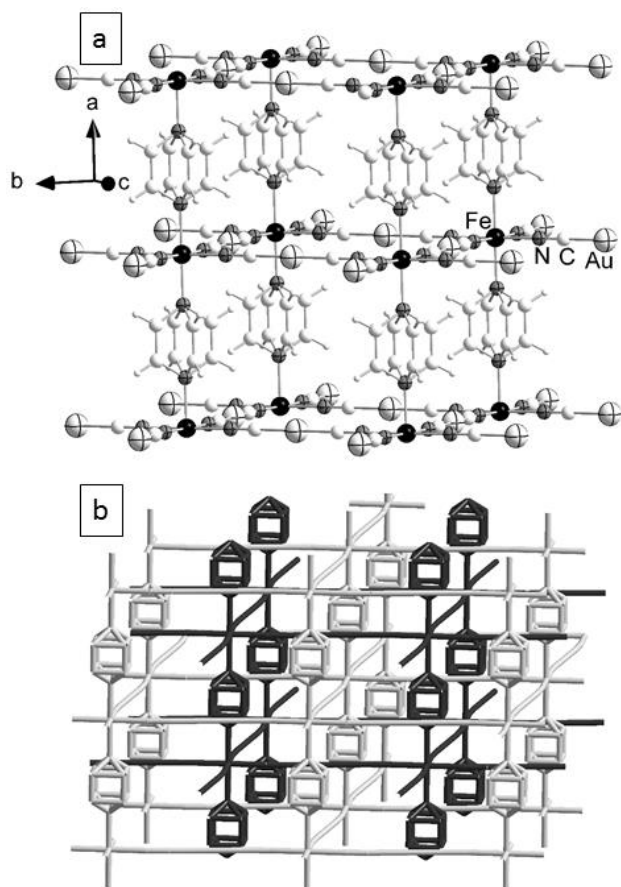


Figure 1. (a) Overall representation of 3D crystal structure of **1**. (b) Interpenetration of two identical networks in **1**.

This interpenetrated network topology is similar to that observed in a silver analogue^[40], and in other cyanoheterometallic complexes with various N-donor ligands (e.g., 3-halopyridines^[41] or pyrimidine^[42]). In contrast, heterocyanometallic frameworks with square planar Ni, Pd and Pt centres have no interpenetration of networks as the voids defined by these tetradentate units are four times smaller than for the bidentate $[\text{Au}(\text{CN})_2]^-$ units. Consequently these $[\text{M}(\text{CN})_4]^{2-}$ -based frameworks frequently present large pores accessible for solvent inclusion.^[38]

Upon heating **1** undergoes a thermally induced SCO, clearly observed using SQUID magnetometry, as shown in **Figures 2** and **S1**. Below 345 K, the complex is in the LS form and is almost diamagnetic ($\chi_{\text{M}}T \sim 0.1 \text{ cm}^3\text{mol}^{-1}\text{K}$). When heated to 367 K it undergoes an abrupt spin transition to the HS form, which is paramagnetic ($\chi_{\text{M}}T \sim 3.34 \text{ cm}^3\text{mol}^{-1}\text{K}$). On cooling the reverse (HS \rightarrow LS) transition occurs at 349 K. A hysteresis loop of 18 K clearly demonstrates the cooperative character of SCO.

Mössbauer spectra (**Figures 3** and **S2**) of the complex in both spin states (LS at 80 and 293 K and HS at 373 K) demonstrate a

complete transition in both directions. The isomer shifts for the LS form (0.391 and 0.345 mm s^{-1} at 80 and 293 K, respectively) are lower than usually observed in clathrate-like SCO compounds (**Table S1**). However, the isomer shift value in the HS form (1.119 mm s^{-1} at 373 K) is somewhat higher than expected. This should be attributed to the relatively stronger π -accepting properties of both pyrazine and cyanoaurate fragments bound to the LS iron ion.

The quadrupole splitting in the LS state (0.261 and 0.259 mm s^{-1} at 80 and 293 K, respectively) and the HS state (1.387 mm s^{-1} at 373 K) are also higher than typical values (**Table S1**). Since the deviation of the FeN_6 fragment from the octahedral geometry is small in both angular ($\Sigma |90^\circ - \Theta_{\text{N-Fe-N}}| = 6.9$ and 5.9° in LS (300 K) and HS (400 K), respectively) and linear ($\text{Fe-N}_{\text{pz}} / \text{Fe-N}_{\text{CN}} = 1.03$ and 0.98 in LS (300 K) and HS (400 K), respectively) measures, the larger electric field gradient is rather driven by the differential ligand field of cyanoaurate and pyrazine ligands.

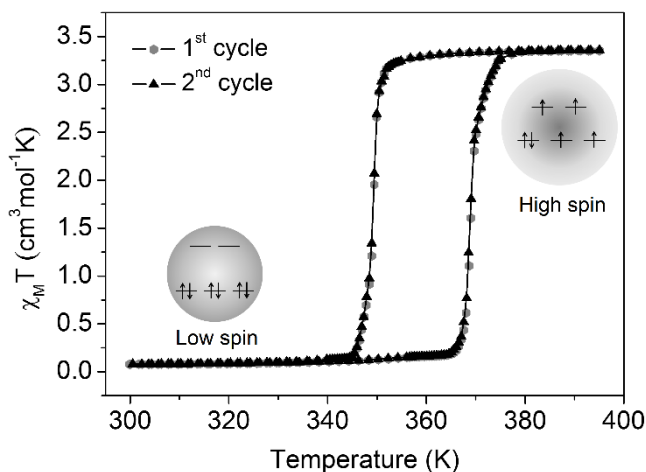


Figure 2. Spin transition in **1** detected in magnetic measurements. Transition from a dia- to a paramagnetic state takes place at 367 K (heating) and 349 K (cooling).

The spin transition has also been observed from DSC measurements, which show characteristic endothermic process upon heating (373 K, 17.1 kJ mol^{-1}) and exothermic process (347 K, 16.0 kJ mol^{-1}) upon cooling (**Figure S3**). The UV-Vis measurements in 200–600 nm region demonstrate a drastic change of the spectrum upon SCO which is related to the complete electronic re-configuration in the framework (**Figure S4**). The absorption band at 294 nm shifts to 279 nm upon LS \rightarrow HS transition. The bands centred at 488 and 524 nm in the LS form disappear upon SCO and a new emerges at 471 nm in the HS state.

The structural evolution of **1** was monitored using single crystal X-ray diffraction at ten temperatures between 300 and 400 K. Inspection of the thermal evolution of unit cell parameters (vide infra) reveals an abrupt, first-order phase transition accompanying the spin transition, with no change in space group. An expansion of the lattice of 6.2 % occurs during the SCO

FULL PAPER

process, albeit with a slight shift in absolute temperature of transition from that determined via other methods.

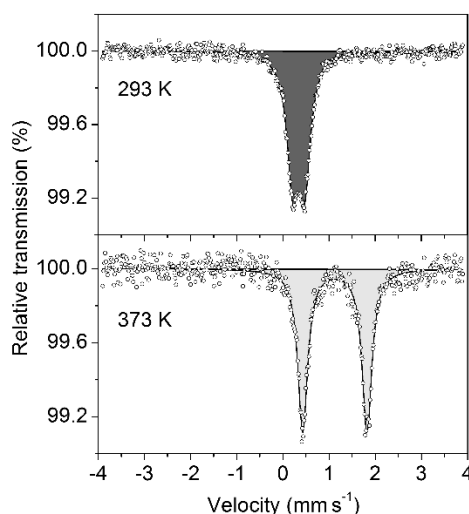


Figure 3. Mössbauer spectra of **1** at 293 and 373 K reveal a complete transition between diamagnetic and paramagnetic states of all iron centres.

More exceptional than this value would imply however is the highly anisotropic nature of the structural changes that occur via a so-called “wine-rack” deformation mechanism.^[43] Superposed sub-lattices of LS and HS forms are shown in **Figure 4**. Deformation along the *a*-axis (5.9 %) is purely related to the Fe-N_{pz} bond length increase (Fe^{HS} (360 K) - N_{pz} = 2.15 Å, Fe^{LS} (340 K) - N_{pz} = 1.988 Å). This increased separation of metal-cyanide layers results in lengthening of inter-gold contacts (Au...Au (LS, 340 K) = 3.389 Å, Au...Au (HS, 360 K) = 3.587 Å), which may represent significant weakening of the aurophilic interaction.

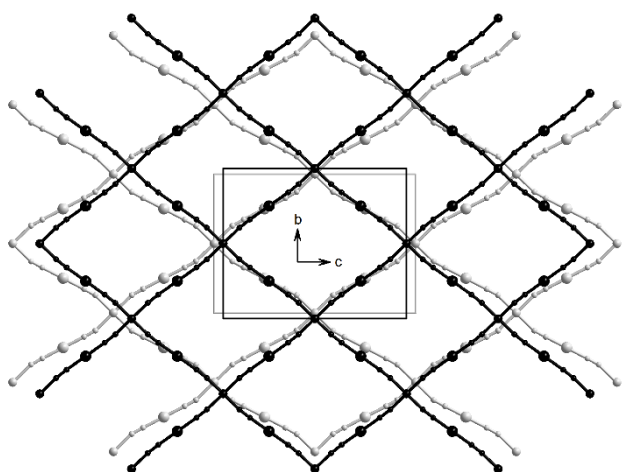


Figure 4. Superposition of LS and HS sub-lattices of **1** demonstrating “wine-rack” deformations accompanying spin transition.

During this deformation, the N_{pz}-Fe-N_{pz} and C-Au-C angles remain unchanged, and the corresponding metal environments are only slightly distorted. The Fe-N_{CN}-C_{CN} fragment appears to be the most flexible unit of the framework – becoming significantly less linear from the LS^{340 K} state (173.8°) to the HS^{360 K} state (166°) (**Table 1**). This bending is mostly responsible for the deformation of the rhombic channels observed during the transition.

The SCO is accompanied by a large expansion in the *c*-direction (10.6 %) and a contraction in the *b*-direction of a similar magnitude (9.6 %). Similar anisotropic expansion behaviour was reported for a molecular complex [Fe(dpp)₂(NCS)₂].py (dpp = dipyrdo[3,2-*a*:2'3'-*c*]phenazine, py = pyridine)^[44], where antagonism between anisotropic mechanical responses to hydrostatic pressure and SCO led to a suppression of the pressure-induced spin transition. More generally, NTE is often related to the structural phase transitions (e.g., in ferroelectrics), electronic phase transitions, magnetostrictive effects, conformational changes in polymers or so-called “transverse thermal motion”.^[45]

Based on the structural information available, such anisotropic deformations during SCO have not yet been observed for Fe(II) heterocyanometallates. However, it is worth to note a negative thermal expansion detected in the HS state of {Fe(3-CNpy)[Au(CN)₂]₂·2/3H₂O} at temperatures above the transition.^[16,46]

The thermal expansion behaviour of the LS and HS forms are broadly similar and they are strongly related to the SCO-associated deformations. The linear $\alpha = dL/(LdT)$ and volume $\beta = dV/(VdT)$ thermal expansion coefficients can be estimated from X-ray diffraction data, despite the small shift in absolute temperature of the transition as determined by magnetometry and DSC.

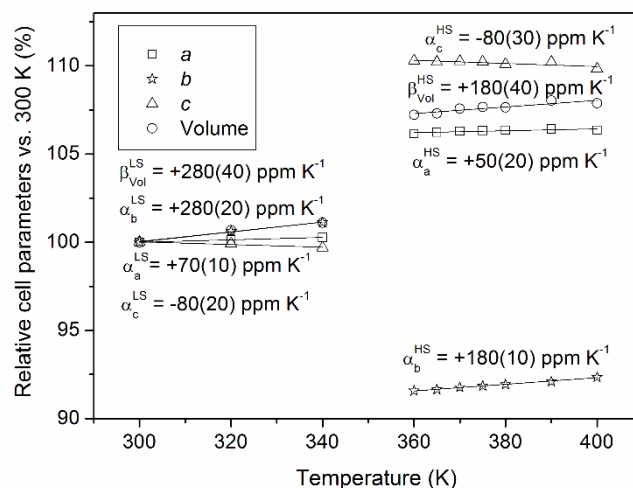


Figure 5. Relative cell parameters of **1** vs. 300 K demonstrating positive and negative thermal and SCO associated expansions.

Table 1. Selected cell parameters, bond lengths and angles for **1** measured at different temperatures within 300 – 400 K region.

T (K)	300	320	340	360	365	370	375	380	390	400
Cell parameters										
a (Å)	6.7584(6)	6.7674(6)	6.7772(7)	7.1740(11)	7.1794(15)	7.1847(13)	7.1857(18)	7.1875(17)	7.1920(19)	7.188(2)
b (Å)	12.7641(12)	12.8436(11)	12.9072(13)	11.6892(14)	11.6983(17)	11.7147(16)	11.725(2)	11.7347(19)	11.756(2)	11.788(3)
c (Å)	15.5641(13)	15.5516(14)	15.5171(17)	17.166(2)	17.154(2)	17.160(2)	17.157(3)	17.135(3)	17.155(3)	17.094(4)
V (Å ³)	1342.6(2)	1351.7(2)	1357.4(2)	1439.5(3)	1440.7(4)	1444.3(4)	1445.5(5)	1445.2(5)	1450.5(6)	1448.4(6)
Bond lengths (Å)										
Fe1-N1	1.919(7)	1.945(11)	1.938(12)	2.17(2)	2.153(17)	2.147(18)	2.130(16)	2.150(16)	2.178(19)	2.155(14)
Fe1-N2	1.968(8)	2.012(15)	1.988(15)	2.15(2)	2.213(17)	2.22(2)	2.17(2)	2.20(2)	2.18(3)	2.21(2)
Bond angles (°)										
C1-N1-Fe1	174.1(7)	174.2(13)	173.8(13)	166(2)	166(2)	158.3(19)	161.1(17)	164.7(19)	166(2)	164.6(15)
N1-C1-Au1	177.1(8)	177.2(15)	177.7(15)	176(3)	176(2)	175(2)	178.1(19)	177(2)	176(3)	178.4(18)

The thermal expansion in the *a*-direction is classical in both spin states ($\alpha_a^{\text{LS}} = +70(10)$ ppm K⁻¹ and $\alpha_a^{\text{HS}} = +50(20)$ ppm K⁻¹). However, the thermal variations along the *b*- and *c*-axes aim to compensate the strain accumulated during the spin transition: comparatively high thermal expansion along the *b*-axis ($\alpha_b^{\text{LS}} = +280(20)$ ppm K⁻¹ and $\alpha_b^{\text{HS}} = +180(10)$ ppm K⁻¹) and a negative thermal expansion along the *c*-axis ($\alpha_c^{\text{LS}} = -80(20)$ ppm K⁻¹ and $\alpha_c^{\text{HS}} = -80(30)$ ppm K⁻¹) are observed. However, all these values should be associated with a narrow temperature region used for the analysis. Thus, a considerable fluctuation of the thermal expansion with temperature was observed in a cyanoheterobimetallic analogue of **1** – Ag₃[Co(CN)₆].^[47] Phase transitions in framework materials with similar “wine-rack” deformation mechanisms have indeed been shown to be considerably higher in magnitude.^[48] However, a considerable feature of the compound discussed here is a narrow temperature region where the phase transition occurs. Expansion/contraction effects that are not directly related to phase transitions (i.e. associated with thermal expansion effects) tend to be significantly smaller.^[49] E.g., exceptional NTE characteristics were obtained for the s-dibenzocyclooctadiene film displaying $\alpha = -1200$ ppm K⁻¹.^[50]

Conclusions

In conclusion, here we describe a new Hofmann clathrate analogue that displays a high temperature spin transition that is unique for this family of materials. The fact that no guest effect is observed and the high reproducibility of the thermal cycle make this compound interesting for application in thermal, pressure, mechanical and other sensors due to the stability of its SCO behaviour. Such cooperative spin transitions are rare at elevated temperatures, making this material interesting for further applications and processing, e.g. towards thin films and

nanoparticles that are well known for Hofmann-clathrate-like SCO compounds.^[9,51] Drastic structural deformations reveal fascinating potential for the development of mechanical sensors and actuators.^[16,17] Spin crossover in analogues with Ag and Cu cyanides, and also with substituted pyrazines, will become a matter of further investigations.

Experimental Section

Synthesis. Single crystals of **1** were obtained by mixing Fe(OTs)₂·6H₂O (50.6 mg, 0.1 mmol), KAu(CN)₂ (57.6 mg, 0.2 mmol) and pyrazine (8 mg, 0.1 mmol) in water (2 ml). A red powder of **1** precipitates immediately and single crystals grow on the tube walls within one week. PXRD and IR of **1** are shown in **Figures S5** and **S6**. Anal. Calcd for C₈H₄N₆Au₂Fe: C, 15.16; N, 13.26; H, 0.64. Found: C, 15.34; N, 13.04; H, 0.63.

XRD measurements. A small piece was cut from a needle-shaped crystal of **1** and placed into the nitrogen stream of an Oxford Cryosystems Cryostream at 300 K. Single crystal data were collected using an Oxford Diffraction Supernova fitted with an EoS detector and Mo-K α radiation ($\lambda = 0.7093$ Å) at ten temperatures between 300 and 400 K. The temperature was ramped at 120 K/hour and allowed to stabilise for 15 minutes at each temperature prior to data collection. For all datasets, the structures were solved with the ShelXS^[52] using Direct Methods and refined with the ShelXL^[52] using Least Squares minimisation. Olex2 was used as an interface to ShelX programs.^[53] All non-hydrogen atoms were refined using an anisotropic model. Hydrogen atoms were placed at calculated positions and refined using a riding model. CCDC deposition numbers are 1422396 – 1422405.

Magnetic susceptibility measurements. Temperature-dependent magnetic susceptibility measurements were carried out with a Quantum-Design MPMS-XL-5 SQUID magnetometer equipped with a 5 T magnet over the temperature range 300–395 K with a heating and cooling rate of 1 K min⁻¹, and a magnetic field of 0.5 T. Diamagnetic correction for the molecule was derived from the Pascal's constants.

FULL PAPER

Mössbauer measurements. ^{57}Fe -Mössbauer spectra were recorded in transmission geometry with a ^{57}Co source in a rhodium matrix using a conventional constant-acceleration Mössbauer spectrometer equipped with either a nitrogen gas-flow cryostat (80 K and 293 K) or oven (373 K). Isomer shifts are given relatively to an $\alpha\text{-Fe}$ foil at ambient temperature. Fits of the experimental Mössbauer data were performed using the Recoil software (Lagarec and Rancourt, Ottawa University).

Acknowledgements

This work was financed by H2020 Marie Skłodowska-Curie Individual Fellowship 659614, the Ukrainian grant 11BF037-03 and the EPSRC grant EP/K012576/1. We acknowledge J. Tapp for the DSC measurements.

Keywords: MOF • spin crossover • structural distortion • cooperativity • magnetic properties

- [1] P. Gütllich, H. A. Goodwin, in *Top. Curr. Chem.*, Springer, **2004**.
- [2] M. A. Halcrow, *Spin-Crossover Materials: Properties and Applications*, John Wiley & Sons, **2013**.
- [3] P. Gütllich, A. B. Gaspar, Y. Garcia, *Beilstein J. Org. Chem.* **2013**, *9*, 342–91.
- [4] S. Brooker, *Chem. Soc. Rev.* **2015**, *44*, 2880–2892.
- [5] J. A. Real, A. B. Gaspar, M. C. Muñoz, *Dalt. Trans.* **2005**, 2062.
- [6] E. Coronado, J. R. Galán-Mascarós, M. Monrabal-Capilla, J. García-Martínez, P. Pardo-Ibáñez, *Adv. Mater.* **2007**, *19*, 1359–1361.
- [7] F. Volatron, L. Catala, E. Rivière, A. Gloter, O. Stéphane, T. Mallah, *Inorg. Chem.* **2008**, *47*, 6584–6586.
- [8] T. Forestier, S. Mornet, N. Daro, T. Nishihara, S. Mouri, K. Tanaka, O. Fouché, E. Freysz, J.-F. Létard, *Chem. Commun.* **2008**, 4327–4329.
- [9] I. Boldog, A. B. Gaspar, V. Martínez, P. Pardo-Ibáñez, V. Ksenofontov, A. Bhattacharjee, P. Gütllich, J. A. Real, *Angew. Chemie Int. Ed.* **2008**, *47*, 6433–6437.
- [10] J. Larionova, L. Salmon, Y. Guari, A. Tokarev, K. Molvinger, G. Molnár, A. Bousseksou, *Angew. Chemie Int. Ed.* **2008**, *47*, 8236–8240.
- [11] I. A. Gural'skiy, V. A. Reshetnikov, A. Szebesczyk, E. Gumienna-Kontecka, A. I. Marynin, S. I. Shylin, V. Ksenofontov, I. O. Fritsky, *J. Mater. Chem. C* **2015**, *3*, 4737–4741.
- [12] C. Faulmann, J. Chahine, I. Malfant, D. de Caro, B. Cormary, L. Valade, *Dalt. Trans.* **2011**, *40*, 2480–2485.
- [13] O. Kahn, C. J. Martínez, *Sci.* **1998**, *279*, 44–48.
- [14] F. Prins, M. Monrabal-Capilla, E. A. Osorio, E. Coronado, H. S. J. van der Zant, *Adv. Mater.* **2011**, *23*, 1545–1549.
- [15] A. Rotaru, J. Dugay, R. P. Tan, I. A. Gural'skiy, L. Salmon, P. Demont, J. Carrey, G. Molnár, M. Respaud, A. Bousseksou, *Adv. Mater.* **2013**, *25*, 1745–1749.
- [16] H. J. Shepherd, I. A. Gural'skiy, C. M. Quintero, S. Tricard, L. Salmon, G. Molnár, A. Bousseksou, *Nat. Commun.* **2013**, *4*, 2607.
- [17] I. A. Gural'skiy, C. M. Quintero, J. S. Costa, P. Demont, G. Molnár, L. Salmon, H. J. Shepherd, A. Bousseksou, *J. Mater. Chem. C* **2014**, *2*, 2949–2955.
- [18] L. Salmon, G. Molnár, D. Zitouni, C. Quintero, C. Bergaud, J.-C. Micheau, A. Bousseksou, *J. Mater. Chem.* **2010**, *20*, 5499–5503.
- [19] G. J. Halder, C. J. Kepert, B. Moubaraki, K. S. Murray, J. D. Cashion, *Sci.* **2002**, *298*, 1762–1765.
- [20] L. G. Lavrenova, O. G. Shakirova, *Eur. J. Inorg. Chem.* **2013**, *2013*, 670–682.
- [21] O. Roubeau, *Chem. - A Eur. J.* **2012**, *18*, 15230–15244.
- [22] A. Grosjean, N. Daro, B. Kauffmann, A. Kaiba, J. F. Letard, P. Guionneau, *Chem. Commun.* **2011**, *47*, 12382–12384.
- [23] A. Grosjean, P. Négrier, P. Bordet, C. Etrillard, D. Mondieig, S. Pechev, E. Lebraud, J.-F. Létard, P. Guionneau, *Eur. J. Inorg. Chem.* **2013**, *2013*, 796–802.
- [24] X. Bao, P.-H. Guo, W. Liu, J. Tucek, W.-X. Zhang, J.-D. Leng, X.-M. Chen, I. Gural'skiy, L. Salmon, A. Bousseksou, et al., *Chem. Sci.* **2012**, *3*, 1629–1633.
- [25] I. Šalitroš, J. Pavlik, R. Boča, O. Fuhr, C. Rajadurai, M. Ruben, *CrystEngComm* **2010**, *12*, 2361–2368.
- [26] R. Boča, M. Boča, L. Dlháň, K. Falk, H. Fuess, W. Haase, R. Jaroščiak, B. Papánková, F. Renz, M. Vrbová, et al., *Inorg. Chem.* **2001**, *40*, 3025–3033.
- [27] R. Boča, F. Renz, M. Boča, H. Fuess, W. Haase, G. Kickelbick, W. Linert, M. Vrbová-Schikora, *Inorg. Chem. Commun.* **2005**, *8*, 227–230.
- [28] Y. Bodenthin, G. Schwarz, Z. Tomkowicz, A. Nefedov, M. Lommel, H. Möhwald, W. Haase, D. G. Kurth, U. Pietsch, *Phys. Rev. B* **2007**, *76*, 064422.
- [29] G. S. Matouzenko, S. A. Borshch, E. Jeanneau, M. B. Bushuev, *Chem. - A Eur. J.* **2009**, *15*, 1252–1260.
- [30] G. Schwarz, Y. Bodenthin, Z. Tomkowicz, W. Haase, T. Geue, J. Kohlbrecher, U. Pietsch, D. G. Kurth, *J. Am. Chem. Soc.* **2011**, *133*, 547–558.
- [31] K. A. Hofmann, F. Höchtlen, *Berichte der Dtsch. Chem. Gesellschaft* **1903**, *36*, 1149–1151.
- [32] M. C. Muñoz, J. A. Real, *Coord. Chem. Rev.* **2011**, *255*, 2068–2093.
- [33] J.-Y. Li, C.-T. He, Y.-C. Chen, Z.-M. Zhang, W. Liu, Z.-P. Ni, M.-L. Tong, *J. Mater. Chem. C* **2015**, *3*, 7830–7835.
- [34] C. Bartual-Murgui, A. Akou, C. Thibault, G. Molnár, C. Vieu, L. Salmon, A. Bousseksou, *J. Mater. Chem. C* **2015**, *3*, 1277–1285.
- [35] D. Aravena, Z. A. Castillo, M. C. Muñoz, A. B. Gaspar, K. Yoneda, R. Ohtani, A. Mishima, S. Kitagawa, M. Ohba, J. A. Real, et al., *Chem. - A Eur. J.* **2014**, *20*, 12864–12873.
- [36] X. Bao, H. J. Shepherd, L. Salmon, G. Molnár, M. L. Tong, A. Bousseksou, *Angew. Chemie - Int. Ed.* **2013**, *52*, 1198–1202.
- [37] Z. Arcis-Castillo, F. J. Muñoz-Lara, M. C. Muñoz, D. Aravena, A. B. Gaspar, J. F. Sánchez-Royo, E. Ruiz, M. Ohba, R. Matsuda, S. Kitagawa, et al., *Inorg. Chem.* **2013**, *52*, 12777–12783.
- [38] M. Ohba, K. Yoneda, G. Agustí, M. C. Muñoz, A. B. Gaspar, J. A. Real, M. Yamasaki, H. Ando, Y. Nakao, S. Sakaki, et al., *Angew. Chemie Int. Ed.* **2009**, *48*, 4767–4771.
- [39] G. Agustí, R. Ohtani, K. Yoneda, A. B. Gaspar, M. Ohba, J. F. Sánchez-Royo, M. C. Muñoz, S. Kitagawa, J. A. Real, *Angew. Chemie Int. Ed.* **2009**, *48*, 8944–8947.
- [40] V. Niel, M. C. Muñoz, A. B. Gaspar, A. Galet, G. Levchenko, J. A. Real, *Chem. - A Eur. J.* **2002**, *8*, 2446.
- [41] M. C. Muñoz, A. B. Gaspar, A. Galet, J. A. Real, *Inorg. Chem.* **2007**, *46*, 8182–8192.
- [42] V. Niel, A. L. Thompson, M. C. Muñoz, A. Galet, A. E. Goeta, J. a. Real, *Angew. Chemie Int. Ed.* **2003**, *42*, 3760–3763.
- [43] A. B. Cairns, A. L. Thompson, M. G. Tucker, J. Haines, A. L. Goodwin, *J. Am. Chem. Soc.* **2012**, *134*, 4454–4456.
- [44] H. J. Shepherd, T. Palamarcu, P. Rosa, P. Guionneau, G. Molnár, J.-F. Létard, A. Bousseksou, *Angew. Chemie Int. Ed.* **2012**, *51*, 3910–3914.
- [45] C. R. Morelock, L. C. Gallington, A. P. Wilkinson, *Chem. Mater.* **2014**, *26*, 1936–1940.
- [46] A. Galet, M. C. Muñoz, V. Martínez, J. A. Real, *Chem. Commun. (Camb.)* **2004**, 2268–2269.
- [47] A. L. Goodwin, M. Calleja, M. J. Conterio, M. T. Dove, J. S. O. Evans, D. A. Keen, L. Peters, M. G. Tucker, *Science* **2008**, *319*, 794–797.
- [48] S. Henke, A. Schneemann, R. A. Fischer, *Adv. Funct. Mater.* **2013**, *23*, 5990–5996.
- [49] M. Azuma, W. Chen, H. Seki, M. Czapski, S. Olga, K. Oka, M. Mizumaki, T. Watanuki, N. Ishimatsu, N. Kawamura, et al., *Nat. Commun.* **2011**, *2*, 347.
- [50] X. Shen, C. Viney, E. R. Johnson, C. Wang, J. Q. Lu, *Nat. Chem.* **2013**, *5*, 1035–1041.
- [51] S. Cobo, G. Molnár, J. A. Real, A. Bousseksou, *Angew. Chemie - Int. Ed.* **2006**, *45*, 5786–5789.
- [52] G. M. Sheldrick, *Acta Crystallogr. Sect. A Found. Crystallogr.* **2008**, *64*, 112–122.

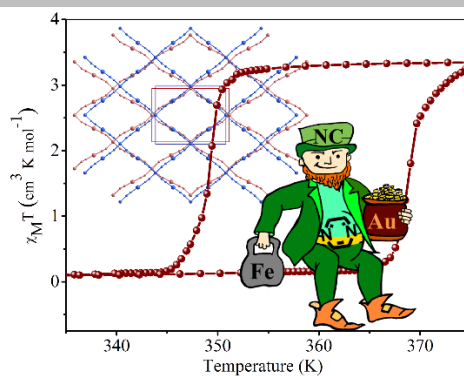
-
- [53] O. V. Dolomanov, L. J. Bourhis, R. J. Gildea, J. A. K. Howard, H. Puschmann, *J. Appl. Crystallogr.* **2009**, *42*, 339–341.

WILEY-VCH

Entry for the Table of Contents

FULL PAPER

A new 3D cyanoheterometallic framework $[\text{Fe}(\text{pz})\{\text{Au}(\text{CN})_2\}_2]$ displays a highly cooperative spin crossover at elevated temperatures. The low spin to high spin transition induces a drastic structural distortion that incorporates large one-directional expansion (10.6 %) and contraction (9.6 %) of the lattice.



Il'ya A. Gural'skiy, Bohdan O. Golub, Sergii I. Shylin, Vadim Ksenofontov, Helena J. Shepherd, Paul R. Raithby, Wolfgang Tremel and Igor O. Fritsky*

Page No. – Page No.

Cooperative High-Temperature Spin Crossover Accompanied by a Highly Anisotropic Structural Distortion